LQG Control of a Two-Wheeled Mobile Pendulum System

Ákos Odry, Ervin Burkus, Péter Odry
Department of Control Engineering and Information Technology
College of Dunaújváros
Dunaújváros, Hungary
E-mail: {odrya, burkus, podry}@mail.duf.hu

***Abstract*—In this paper, the linear-quadratic-Gaussian control of a mechatronic system will be studied. The mechatronic system is a special mobile robot (called two-wheeled mobile pendulum) having two-wheels, two contact points with the supporting surface and its center of mass is located under the wheel axis. Due to the mechanical structure, the inner body (which acts as a pendulum between the wheels) tends to oscillate during the translational motion of the robot, thus the application of modern control methods is essential in order to stabilize the dynamical system. In the first part of the paper, the mechatronic system and the corresponding mathematical model are introduced, while in the second part different controllers are designed for the plant. The achieved control performances are analyzed based on simulation and implementation results.**

Keywords-LQG control; Kalman-filter; mobile robot; self-balancing robot; future transportation system

I. INTRODUCTION

The linear-quadratic-Gaussian (LQG) technique is a beloved method in the control of dynamical systems since it provides the optimal state feedback gain based on the well-developed mathematical algorithm [1]. Numerous researches have been dealt with its application and control performance in real embedded environments such as references [2] - [9]. Divelbiss and Wen [2] presented their experimental results of the tracking control of a car-trailer system, where linear quadratic regulator was used to track the trajectory. Ji and Sul [4] proposed an LQG-based speed control method for torsional vibration suppression in a 2-mass motor drive system, which gave satisfying performance and robust behavior against parameter variations. Bouabdallah, Noth and Siegwart [5] compared the control performances of the PID and linear-quadratic (LQ) techniques applied to an autonomous four-rotor micro helicopter, and emphasized that the control performance of the later technique was influenced by model imperfections. Recent efforts broaden further the set of experimental research results regarding the LQG control, including the control of inverted pendulum type assistant robot [6], self-balancing unicycle robot [7], unmanned helicopter in an uncertain environment [8], inverted pendulum system [9], and quadrotors [3] as well. All the mentioned papers show that the LQG technique have proved its competitive performance in the control of dynamical systems.

Our research goal is to analyze critical balance tasks through the design, optimization and validation of modern control methods. Thus, as a first step, the design and implementation of the well-known LQG controller had been performed, where the resultant control performances form the initial results of our research analysis. These initial results can be used in the design optimization or in the comparison with other control methods (such as fuzzy control), which is left for another publication.

On the other hand, it can be observed that nowadays technological efforts focus on the development and application of modern control solutions by which mechanical or other kind of anomalies are compensated in dynamical systems (the result of such aspirations is for example the transportation vehicle Segway). Since the two-wheeled mobile pendulum system shall be stabilized by feedback in order to achieve translational motion, we also strengthen and develop this tendency by the analysis and design of modern, optimized control solutions for the plant.

The remainder of this paper is organized as follows. In section II, the mechatronic structure of the robot is introduced, while in section III, the corresponding nonlinear mathematical is derived. In section IV, the control tasks and the LQG control method are reviewed. From section V, the control strategies are elaborated, namely, in section V, the anti-sway speed control-, while in section VI, the balance control of the robot are designed with simulation results. Section VII deals with the state estimation, while in section VIII, the application of the complete LQG control strategies is described. The implementation results of the elaborated control strategies are given in section IX. Section X contains the conclusions and the future work recommendations.

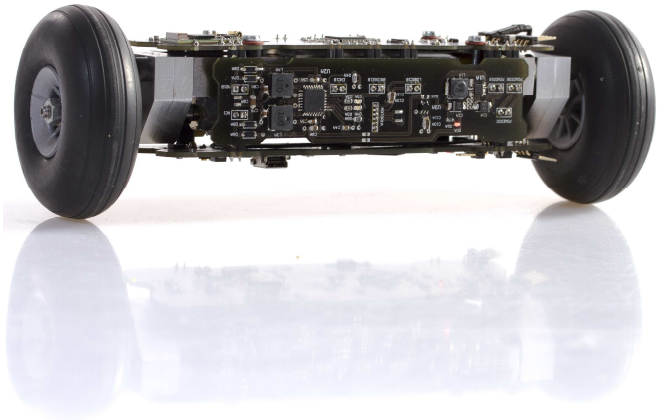

Figure 1. Photograph of the fabricated robot.

 ISBN: 978-1-61208-437-4

II. THE FABRICATED MECHATRONIC SYSTEM

The mechatronic system is a special mobile robot (called two-wheeled mobile pendulum) consisting of two wheels and a steel inner body (chassis). The wheels are actuated through DC motors that are attached to the body. As it can be seen in Figure 1, the diameter of the wheels is bigger than the diameter of the intermediate body, thus the robot has only two contact points with the supporting surface. Due to this mechanical structure, the inner body behaves as a pendulum between the stator and rotor of the applied DC motors, and tends to oscillate when the robot performs translational motion.

Since the location of the center of mass of the robot can be under and above the wheel axis, two equilibrium points can be distinguished. Namely, the robot stays around its stable equilibrium point when the center of mass is located under the wheel axis. Therefore, around this state the translational motion of the robot is affected by the damped oscillation of the inner body. On the other hand, the robot is operated around its unstable equilibrium point when the center of mass is stabilized above the wheel axis. Around the unstable equilibrium point, the robot simultaneously performs translational motion and balances its inner body, which acts as an inverted pendulum. For video demonstration see the website [10].

The electronic construction is built around two 16-bit ultra-low-power Texas Instruments MSP430F2618 microcontrollers (hereinafter MCU1 and MCU2). The applied sensors are summarized in Table 1. The actuators are 3V geared DC micromotors (type: 1024N003S) manufactured by Faulhaber. The motors are driven with pulse width modulation (PWM) signals through Texas Instruments DRV592 drivers. The electronic system is supplied from stabilized 3.3V, the source is a 1 cell lithium-polymer (Li-Po) battery. A 16 MHz quartz oscillator is used as the system clock.

Similar construction was built at the McGill University's Centre for Intelligent Machines [11]. It was proven that the two contact point construction is characterized by the so called quasiholonomic property that eases the control of nonholonomic systems. Another corresponding two contact point construction is the electric diwheel built by the School of Mechanical Engineering at the University of Adelaide [12].

III. MATHEMATICAL MODEL

To be able to efficiently design the control algorithms of the system, its mathematical model has to be obtained first. Most of the electrical and mechanical parameters that characterize the robot dynamics (such as wheel radius or resistance of the motor) are quite accurately known from direct measurements, datasheets or from calculations performed by Solidworks, the rest of the parameters were experimentally tuned based on the measurements.

We indicate with $\theta_1$and θ_2 the angular displacements of the wheels, while with θ_3 the inclination angle of the pendulum (inner body). The parameters that characterize the robot are summarized in Table 2 in the appendix. The following notations will be also used: $\dot{\theta}$ as the mean value of $\dot{\theta}_1$and $\dot{\theta}_2$, $\dot{\psi}$ as the change of yaw angle of the robot, and $\dot{s}$ as the linear speed of the robot, i.e., $\dot{\theta} = (\dot{\theta}_1 + \dot{\theta}_2)/2$, $\dot{\psi} = r(\dot{\theta}_2 - \dot{\theta}_1)/d$, and $\dot{s} = r\dot{\theta}$.

TABLE I. THE APPLIED SENSORS IN THE EMBEDDED ELECTRONICS

Sensor	Manufacturer	Type
Accelerometer	STMicroelectronics	LIS331DL
Gyroscope	STMicroelectronics	L3G4200D
Current sensors	Texas Instruments	INA198
Incremental encoders	Faulhaber	PA2-100

The motion of the system was determined by the help of the Lagrange equations [13], which lead us to the following equations of motion of the mechanical system [14]:

$$M(q)\ddot{q} + V(q,\dot{q}) = \tau_a - \tau_f, \tag{1}$$

where $M(q)$ denotes the 3-by 3 symmetric and positive definite inertia matrix, $V(q,\dot{q})$ denotes the 3-dimensional vector term including the Coriolis and centrifugal force terms and also the potential (gravity) force term.

The Lagrange function and the exact elements of the matrices in (1) are described in the appendix. For the vector of generalized coordinates $q = (\theta_1, \theta_2, \theta_3)^T$ was chosen, since it contains the minimum number of independent coordinates that define the configuration of the system. The generalized external forces in (1) consist of the torques τ_a that are produced by the motors and the effect of friction τ_f that is modeled in the system [14]. The torques τ_a are described by the differential equation (2) where the input voltages and currents of the motors are denoted with $u = (u_1, u_2)^T$ and $I = (I_1, I_2)^T$.

$$\dot{I} = \frac{1}{L}\left(u - k_E k \begin{bmatrix} 1 & 0 & -1 \\ 0 & 1 & -1 \end{bmatrix} \dot{q} - RI\right),$$
$$\tau_a = k_M k \begin{bmatrix} 1 & 0 \\ 0 & 1 \\ -1 & -1 \end{bmatrix} I. \tag{2}$$

Regarding the effect of friction τ_f, only viscous frictions were assumed. Namely, viscous friction was modelled at the bearings and between the wheels and the supporting surface:

$$\tau_f = \begin{bmatrix} b + f_v & 0 & -b \\ 0 & b + f_v & -b \\ -b & -b & 2b \end{bmatrix} \dot{q}. \tag{3}$$

Based on (1) the state-space representation of the two-wheel inverted pendulum system is obtained. With the state vector $x = (q, \dot{q}, I)^T$ the state-space equation [14]:

$$\dot{x}(t) = h(x,u),$$
$$h(x,u) = \begin{bmatrix} \dot{q} \\ M(q)^{-1}\left(\tau_a - \tau_f - V(q,\dot{q})\right) \\ \frac{1}{L}\left(u - k_E k \begin{bmatrix} 1 & 0 & -1 \\ 0 & 1 & -1 \end{bmatrix} \dot{q} - RI\right) \end{bmatrix}, \tag{4}$$
$$y(t) = x(t).$$

Remark: In the simulation environment the state-space equation (4) was implemented, however during the design of the LQG controllers the 6-dimensional version defined by the state vector $x = (q, \dot{q})^T$ was used. This outcome was chosen because the current measurements were that noisy that the states $I = (I_1, I_2)^T$ could not be used in the feedback. The 6-dimensional model is derived by neglecting the inductance L of the motors.

IV. CONTROL TASKS

Two control tasks were investigated in the analysis, namely the balance control and the anti-sway control of the plant. Therefore, around the stable equilibrium point the speed control of the robot had been chosen as control task, where the implemented controller shall minimize the resulting oscillation of the inner body. While around the unstable equilibrium point the position control of the robot had been chosen as control task, where the implemented controller shall stabilize the inner body during the translational motion.

A. LQ control

The linear-quadratic control addresses the issue of achieving a balance between good system response and control effort [1]. It is based on a developed mathematical algorithm, which results the optimal state-feedback gain K. The feedback gain K minimizes the quadratic cost function

$$J(x,u) = \frac{1}{2}\sum_{k=0}^{N-1}(x_k^T Q x_k + u_k^T R u_k) + \frac{1}{2}x_N^T Q x_N, \quad (5)$$

where $x \in \mathbb{R}^n$ and $u \in \mathbb{R}^m$ are the state and input of the system described by its state-space equation, while $Q = Q^T \in \mathbb{R}^{n\times n}, Q \geq 0$ and $R \in \mathbb{R}^{m\times m}, R > 0$ are weighting matrixes. According to the LQR method, the state feedback matrix is given by $K = (R + B^T P B)^{-1} B^T P A$, where $P = P^T \geq 0$ is the unique solution of the Control Algebraic Riccati Equation (CARE). The optimal state-feedback $u_k = -Kx_k$ ensures the asymptotic stability of the closed loop system. The feedback matrix K is calculated by the built-in Matlab function lqrd(A,B,Q,R,Ts).

B. Reference tracking

Since the LQ control defined by the objective function (5) drives the system from the initial state x_0 to the state $x_d = 0$, the control structure shall be extended with the reference tracking matrixes:

$$\begin{pmatrix} N_x \\ N_u \end{pmatrix} = \begin{bmatrix} A - I & B \\ C & 0 \end{bmatrix}^{-1} \begin{pmatrix} 0_{n\times m} \\ I_m \end{pmatrix}, \quad (6)$$

where 0 and I are the zero and identity matrixes respectively (the sizes are given in the subscript).

C. LQG control

In the development of the optimal LQ control strategy it is assumed the state variables are measurable, and the system is not disturbed by either internal or external noises. However in practice the opposite situation is quite common, namely, that a part of the state vector is too noisy to use directly in the feedback. The LQG strategy provides optimal control gain to stochastic, noisy systems by minimizing the expected value of the quadratic objective function (5).

Based on the separation principle the LQG control strategy is given by the state-feedback $u_k = -K\hat{x}_k$, where K is the optimal control gain determined by the LQR algorithm, while $\hat{x}_k$ state vector consists of the original states (those states of x_k that were not noisy) and the Kalman-filter based estimation of the noisy states. Let us denote the unmeasurable or noisy states with ξ, than the corresponding noisy linear system can be given by:

$$\begin{aligned} \xi_{k+1} &= \Phi\xi_k + \Gamma\rho_k + v_k, \\ \gamma_k &= \mathrm{P}\xi_k + z_k, \end{aligned} \quad (7)$$

where the process and measurement noises are indicated with v and z respectively, and according to the stochastic hypothesis these noises are uncorrelated and their mean value is zero. In this case the Kalman-filter algorithm provides the optimal estimation $\hat{\xi}$ of the state ξ, i.e., $E[\xi_k - \hat{\xi}_k] = 0$ and $E\left[(\xi_k - \hat{\xi}_k)(\xi_k - \hat{\xi}_k)^T\right] \to \inf$. The estimation algorithm can be found in [15].

Therefore, the design steps are the following: i.) Linearization of the mathematical model around an equilibrium point, ii.) Controllability analysis, iii.) Specification of the weighting matrixes, iv.) Calculation of the optimal control gain K, v.) Identification of the noisy states, vi.) Specification of the noise covariance parameters of the filter, vii.) State estimation by Kalman filter and viii.) Application of the state feedback strategy $u_k = -K\hat{x}_k$.

V. CONTROL STRATEGY AROUND THE STABLE EQUILIBRIUM POINT

Around the stable equilibrium point the anti-sway speed control of the robot is elaborated.

A. Elaboration

The linear state space equation is given by the linearization of (4) around the equilibrium $(x_e, u_e) = (0,0)$:

$$\dot{x} = \underbrace{\left(\frac{\partial h}{\partial x}\right)_{(x_e,u_e)}}_{A_s} x(t) + \underbrace{\left(\frac{\partial h}{\partial u}\right)_{(x_e,u_e)}}_{B_s} u(t), \quad (8)$$

where the subscript s refers to the stable equilibrium point. In order to reduce the complexity of implementation the $\tilde{x} = Tx = (s, \theta_3, \dot{s}, \dot{\theta}_3, \psi, \dot{\psi})$ coordinate transformation is applied. The resulting state-space representation is given by:

$$\begin{aligned} \dot{\tilde{x}} &= \begin{bmatrix} 0_{2\times2} & I_2 & 0_{2\times2} \\ \tilde{A}_{s,21} & \tilde{A}_{s,22} & 0_{2\times2} \\ 0_{2\times2} & 0_{2\times2} & \tilde{A}_{s,33} \end{bmatrix}\tilde{x} + \begin{bmatrix} 0_{2\times2} \\ \tilde{B}_{s,2} \\ \tilde{B}_{s,3} \end{bmatrix} u, \\ y &= \begin{bmatrix} 0_{2\times2} & \tilde{C}_{s,2} & \tilde{C}_{s,3} \end{bmatrix}\tilde{x}, \end{aligned} \quad (9)$$

where the block matrices are described in the appendix.

The controllability matrix [1] is given by $M_c = [B \quad AB \quad \dots \quad A^5B]_{(\tilde{A}_s,\tilde{B}_s)}$ and the evaluation of its rank results $\operatorname{rank} M_c = 4$. Therefore, according to the Kalman rank condition for controllability (KRCC) the system (9) is not controllable, since the dimension of the state vector is $\dim \tilde{x} = 6$. The non-controllable states of $\tilde{x}$ are the position s and the orientation ψ.

Thus, a new coordinate transformation $z = T_{C\bar{C}}\tilde{x}$ is defined, such that $T_{C\bar{C}} = (T_C, T_{\bar{C}})$ is a basis for $\mathbb{R}^6$, furthermore the columns of T_C form the basis for the controllable subspace, $\dim T_C = 6 \times 4$ and $\dim T_{\bar{C}} = 6 \times 2$. As a consequence of the definition, the state vector $z = (z_C, z_{\bar{C}})^T$ is clearly devided into two parts, namely $z_C = \left(\theta_3, \dot{s}, \dot{\theta}_3, \dot{\psi}\right)^T$ denotes the controllable states, while $z_{\bar{C}} = (s, \psi)^T$ contains uncontrollable ones, and the state-space representation becomes

$$\dot{z} = \begin{bmatrix} A_C & A_{C\bar{C}} \\ 0 & A_{\bar{C}} \end{bmatrix} z(t) + \begin{bmatrix} B_C \\ 0 \end{bmatrix} u(t), \qquad y = [C_C \quad C_{\bar{C}}] z(t). \tag{10}$$

The LQ strategy is elaborated by using the controllable subsystem (A_C, B_C). The weighting matrixes $Q = \operatorname{diag}(Q_{ii})$ and $R = \operatorname{diag}\left(\mathrm{R}_{jj}\right)$ were defined based on the Bryson's rule, where $Q_{11} = (15 \cdot \pi/180)^{-2}$, $Q_{22} = (0.08)^{-2}$, $Q_{33} = (50 \cdot \pi/180)^{-2}$, $Q_{44} = (50 \cdot \pi/180)^{-2}$ and $R_{11} = R_{22} = 3^{-2}$ were chosen. Solving the CARE the optimal control gain:

$$K^s = \begin{bmatrix} -1.75 & -1.26 & -0.2 & -0.61 \\ -1.75 & -1.26 & -0.2 & +0.61 \end{bmatrix}, \tag{11}$$

while the reference tracking matrixes are

$$N_x^s = \begin{bmatrix} -0.41 & 0 \\ 1 & 0 \\ 0 & 0 \\ 0 & 1 \end{bmatrix}, \quad N_u^s = \begin{bmatrix} 4.28 & -0.37 \\ 4.28 & +0.37 \end{bmatrix}. \tag{12}$$

B. Simulation results

Simulation of the proposed control strategy was done in MATLAB Simulink environment. The simulation results of the closed loop behavior is depicted in Figure 2.

From the top, the first is the linear speed $\dot{s}$ of the robot, the second is the change of yaw $\dot{\psi}$, the third is the resulting oscillation θ_3 of the inner body, while the last one is the applied voltage to the motors. The following reference signals were applied:

- $\dot{s}_d = \{0.4, 0, -0.2, 0\}$ [m/s],
- $\dot{\psi}_d = \{0.5, 0, -1.2, 0\}$ [rad/s].

The simulation results show that the applied control strategy satisfies the requirements, since the controller simultaneously ensures the speed control and the suppression of the inner body oscillations. The dynamics of the plant was sampled at fixed $f_s = 100\ Hz$, which equals to the sampling frequency of the applied sensors.

VI. Control Strategy Around The Unstable Equilibrium Point

Around the unstable equilibrium point the position control of the robot and the stabilization of its inner body is elaborated.

A. Elaboration

The state space equation is given by the linearization of (4) around $x_e = (0,0,\pi,0,0,0)^T$ and $u_e = 0$:

$$\dot{x} = \underbrace{\left(\frac{\partial h}{\partial x}\right)_{(x_e,u_e)}}_{A_u} x(t) + \underbrace{\left(\frac{\partial h}{\partial u}\right)_{(x_e,u_e)}}_{B_u} u(t), \tag{13}$$

where the subscript u refers to the unstable equilibrium point. Again, the coordinate transformation $\tilde{x} = Tx = \left(s, \theta_3, \dot{s}, \dot{\theta}_3, \psi, \dot{\psi}\right)$ is applied:

$$\dot{\tilde{x}} = \begin{bmatrix} 0_{2\times2} & I_2 & 0_{2\times2} \\ -\tilde{A}_{s,21} & \tilde{A}_{s,22} & 0_{2\times2} \\ 0_{2\times2} & 0_{2\times2} & \tilde{A}_{s,33} \end{bmatrix} \tilde{x} + \begin{bmatrix} 0_{2\times2} \\ \tilde{B}_{s,2} \\ \tilde{B}_{s,3} \end{bmatrix} u, \qquad y = \begin{bmatrix} \tilde{C}_{s,2} & 0_{2\times2} & \tilde{C}_{u,3} \end{bmatrix} \tilde{x}, \tag{14}$$

where the block matrix $\tilde{C}_{u,3} = \begin{bmatrix} 0 & 0 \\ 1 & 0 \end{bmatrix}$.

According to KRCC the system (14) is controllable, since $\operatorname{rank} M_c|_{(\tilde{A}_u,\tilde{B}_u)} = 6 = \dim \tilde{x}$. Similarly to the stable equilibrium point, the weighting matrixes were specified by the help of the Bryson's rule. Therefore, $Q = \operatorname{diag}(Q_{ii})$ and $R = \operatorname{diag}\left(\mathrm{R}_{jj}\right)$, where $Q_{11} = 0.1^{-2}$, $Q_{22} = (10 \cdot \pi/180)^{-2}$, $Q_{33} = (0.15)^{-2}$, $Q_{44} = (150 \cdot \pi/180)^{-2}$, $Q_{55} = (10 \cdot \pi/$

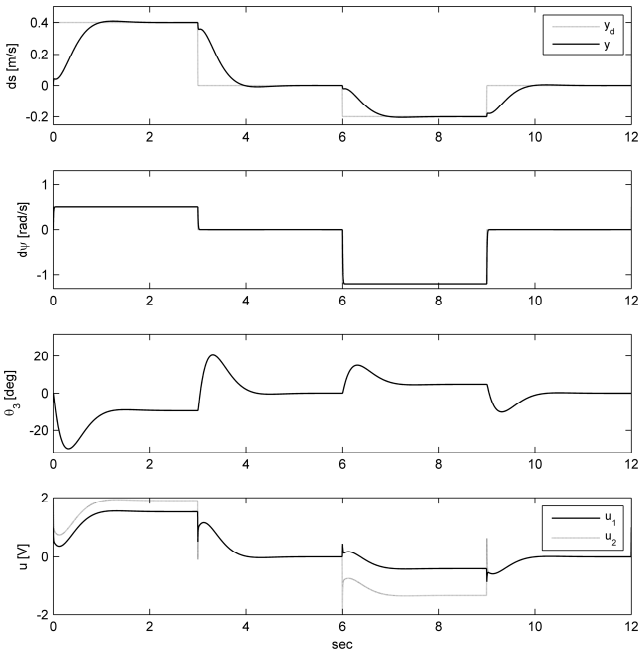

Figure 2. Simulation results. Control performance around the stable equilibrium point.

$180)^{-2}$, $Q_{66} = (45 \cdot \pi/180)^{-2}$, and $R_{11} = R_{22} = 3^{-2}$. Solving the CARE the optimal feedback gain $K^u = (K_1^u, K_2^u)$ takes the form (15), while the reference tracking matrices are given by (16):

$$K_1^u = \begin{bmatrix} -7.46 & -5.47 & -11.1 & -0.28 \\ -7.46 & -5.47 & -11.1 & -0.28 \end{bmatrix}, \quad K_2^u = \begin{bmatrix} -4.35 & -0.634 \\ +4.35 & +0.634 \end{bmatrix}, \tag{15}$$

$$N_x^u = \begin{bmatrix} 1 & 0 & 0 & 0 & 0 & 0 \\ 0 & 0 & 0 & 0 & 1 & 0 \end{bmatrix}^T, \quad N_u^u = 0_{2\times 2}. \tag{16}$$

B. Simulation results

Simulation results are shown in Figure 3. From the top, the first is the linear position s of the robot, the second is the yaw angle ψ, the third is the tilt angle θ_3 of the inner body, while the last one is the applied voltage to the motors. The simulation was started with the following initial conditions: $x_0 = \left[0.05, 8 \cdot \frac{\pi}{180}, 0, 0, 20 \cdot \frac{\pi}{180}, 0\right]$. It can be seen, that the calculated optimal feedback gain asymptotically stabilizes the closed loop system, and both the stabilization of the inner body and the position control is ensured. The following reference signals were applied in the simulation: $s_d = \{0, 0.1, -0.05, 0\}$ [m] and $\psi_d = \{0, 1.5, 0, -0.7\}$ [rad].

VII. State Estimation with Kalman-filter

The Kalman filter is used to estimate the tilt angle θ_3 of the inner body (second element of $\tilde{x}$). Since the accelerometer measures the projection of gravity vector onto its axes, the angle is given by $\theta_{3,acc} = \operatorname{atan}\left(\frac{a_y}{a_x}\right)$ [16]. Unfortunately,

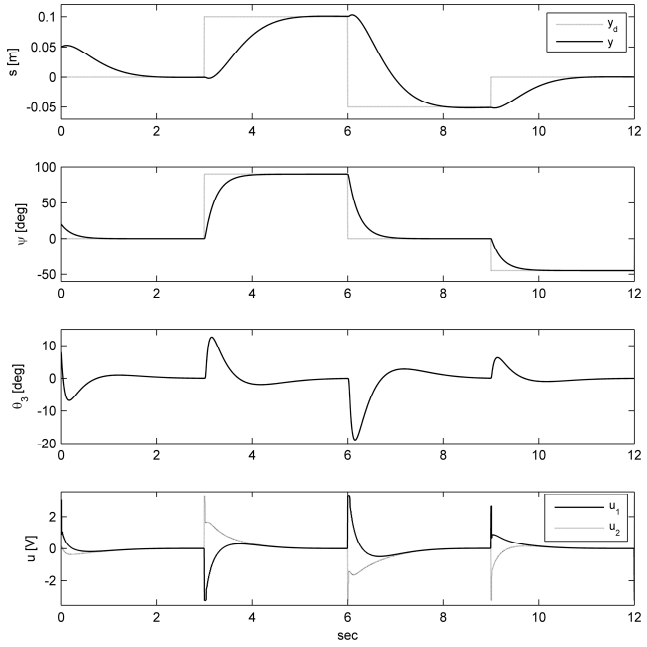

Figure 3. Simulation results. Control performance around the unstable equilibrium point.

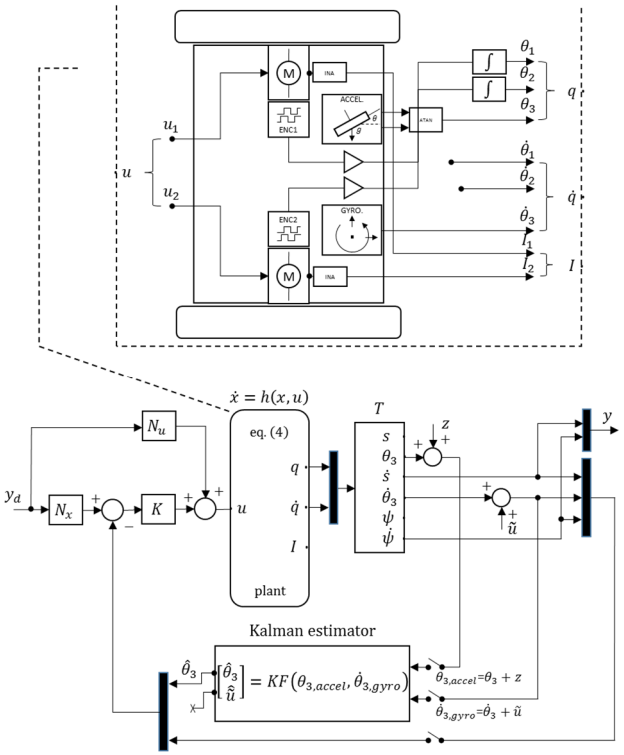

Figure 4. Detailed LQG control structure.

$\theta_{3,acc}$ is very noisy, in the most control methods useless and it can't be considered as an accurate derived quantity at high frequency rates of rotation, because the accelerometer measures both the static acceleration of the gravity and the dynamic acceleration of the robot as well. Thus, it is common to consider the gyroscope and accelerometer as a noisy linear system and use the Kalman filter to estimate the state vector. The corresponding state-space equation is given by:

$$\xi_{k+1} = \begin{bmatrix} 1 & -1/f_s \\ 0 & 1 \end{bmatrix} \xi_k + \begin{bmatrix} 1/f_s \\ 0 \end{bmatrix} \rho_k + v_k \qquad \gamma_k = [1 \quad 0]\xi_k + z_k, \tag{17}$$

where the state vector $\xi = (\theta_3, \tilde{u})^T$ consists of the inclination angle θ_3[rad], and the bias of the gyroscope $\tilde{u}$[rad/s].

Furthermore, the input of the linear system is the angular velocity $\rho = \dot{\theta}_3$[rad/s] (measured by the gyroscope), while the output of the system is the derived angle $\gamma = \theta_{3,acc}$[rad] from the pure accelerometer measurements. The covariance matrixes that characterize the measurement and state noises were defined based on offline measurements.

VIII. The LQG Control Structures

According to the separation principle the LQG control strategies are elaborated as follows. Around the stable equilibrium point the state feedback $u_k = -K(\hat{\theta}_3, \dot{s}, \dot{\theta}_3, \dot{\psi})$ ensures asymptotic stability of the closed loop system, where $\hat{\theta}_3$ denotes the Kalman-filter based estimation of the tilt angle of the inner body and the optimal control gain K is defined by (11). The detailed control structure is depicted in Figure 4.

While around the unstable equilibrium point, the state feedback $u_k = -K(s, \hat{\theta}_3, \dot{s}, \dot{\theta}_3, \psi, \dot{\psi})$ provides the stabilization of the system, where the optimal control law is defined by (15) (the figure of the control structure is neglected since it's almost the same as Figure 4).

IX. IMPLEMENTATION RESULTS

The control algorithm was coded in C language. MCU2 was programmed to work as an inertial measurement unit (IMU). Its main task is to read the data of sensors (from accelerometer and gyroscope through SPI peripheral), and send a package consisting of $\theta_{3,acc}$, $\dot{\theta}_3$, and $\hat{\theta}_3$ to MCU1 continuously (in every $T_s = 10\,ms$), where $\theta_{3,acc}$ indicates the inclination angle determined based on the pure accelerations measured by the accelerometer, $\dot{\theta}_3$ denotes the angular velocity of the pendulum measured by the gyroscope, while $\hat{\theta}_3$ indicates the Kalman estimation of the inclination angle. MCU1 executes the chosen control algorithm based on the collected measurements. It receives the package $(\theta_{3,acc}, \dot{\theta}_3, \hat{\theta}_3)$ from MCU2 and extends it with the instantaneous position and velocity of the robot $(s, \dot{s})$ based on the measurements collected from the incremental encoders. Once the measurements are updated the chosen control algorithm updates the duty cycle of the PWM generator. Furthermore, the measurements are sent through the Bluetooth module with the frequency $f_s = 100Hz$. A GUI written in MATLAB records the measurements.

The control performance was tested in different environments, i.e., both static and dynamic behavior of the chosen control algorithm. During the test of the dynamic behavior the robot was pushed away from its stable position.

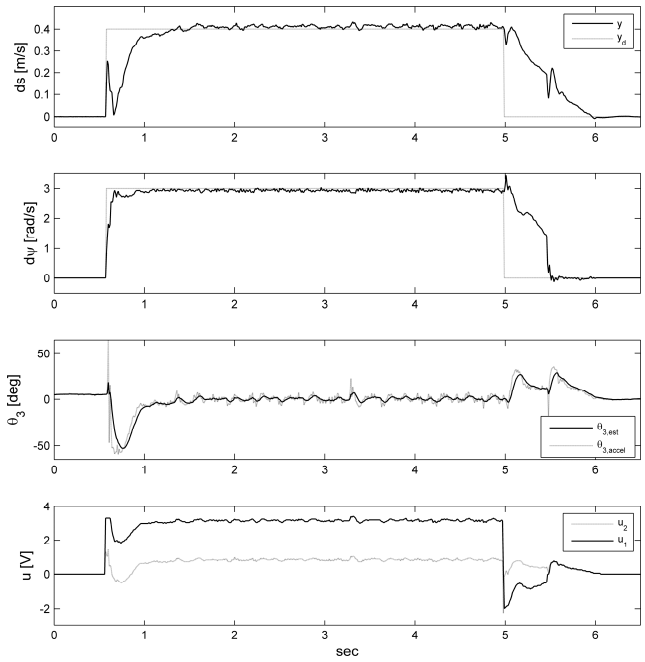

Figure 5. Implementation results. Control performance around the stable equilibrium point. Reference signals: $\dot{s}_d = 0.4$ [m/s], $\dot{\psi}_d = 3$ [rad/s].

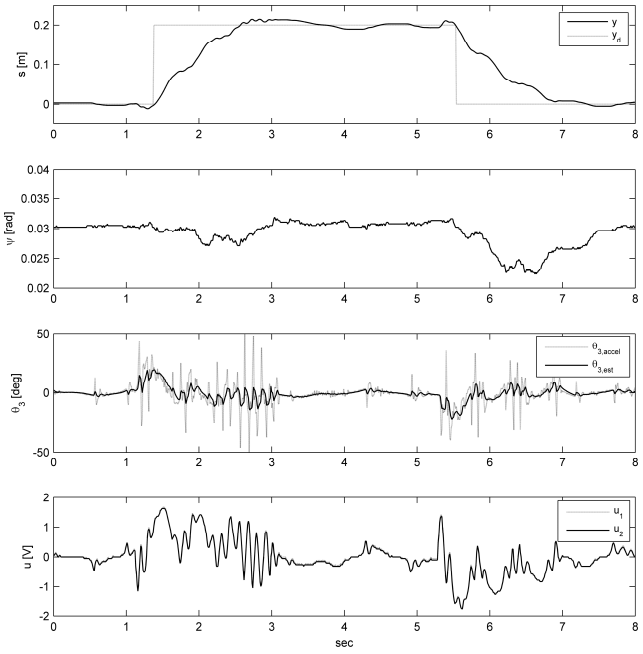

Figure 6. Implementation results. Control performance around the unstable equilibrium point. Reference signal: $s_d = 0.2$ [m].

A. Control around the stable equilibrium point

The control performance is depicted in Figure 5. From the top, the first is the linear speed $\dot{s}$, the second is the change of yaw $\dot{\psi}$, the third is the angle of the inner body θ_3, while the last one is the applied voltage. It can be seen that the implemented LQG control strategy successfully suppressed the oscillation of the inner body and ensured the speed control of the robot as well.

B. Control around the unstable equilibrium point

The implementation results are depicted in Figure 6, 7 and 8. From the top, the first is the linear position s, the second is the yaw angle ψ, the third is the angle of the pendulum θ_3, while the last one is the applied voltage. Based on the measurements, it can be concluded that the elaborated LQG control strategy ensured both the stabilization of the inner body around the unstable equilibrium point, and the position control of the robot as well.

In Figure 6 $s_d = 0.2$ [m] reference signal was applied and the stabilization took approximately 2.5 seconds. The noisy measurements of the tilt range and the importance of the Kalman filtration can be also observed in the figures, since ± 50 [°] oscillations were not present evidently during the balancing. The static behavior of the balancing was also investigated. It can be seen in Figure 7 that if there is no external perturbation the balancing range is in ± 5 [°], while the position control tracks the reference with ± 5 [mm] error.

Finally, the dynamic behavior of the implemented control strategy was also tested on the robot, i.e., the robot was pushed away several times from its equilibrium state (the external perturbations are indicated with arrows). As it can be seen in Figure 8, both the balance and the stabilization of the robot

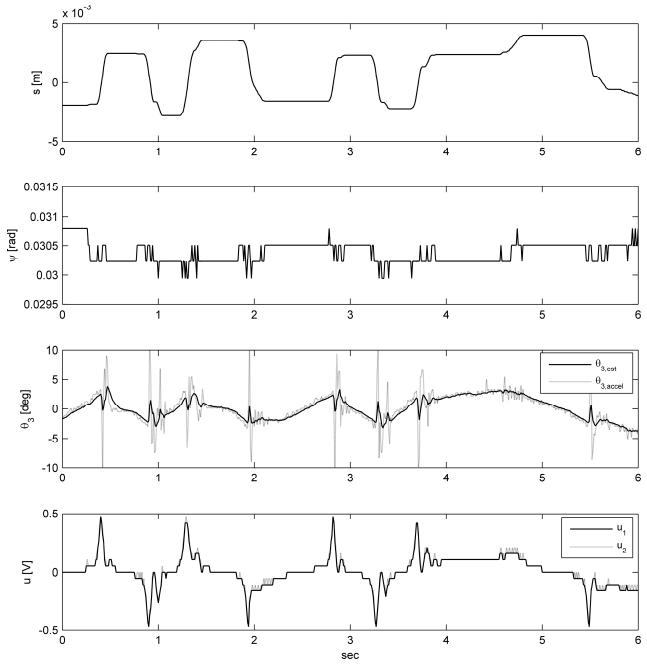

Figure 7. Implementation results. Control performance around the unstable equilibrium point. Static behavior.

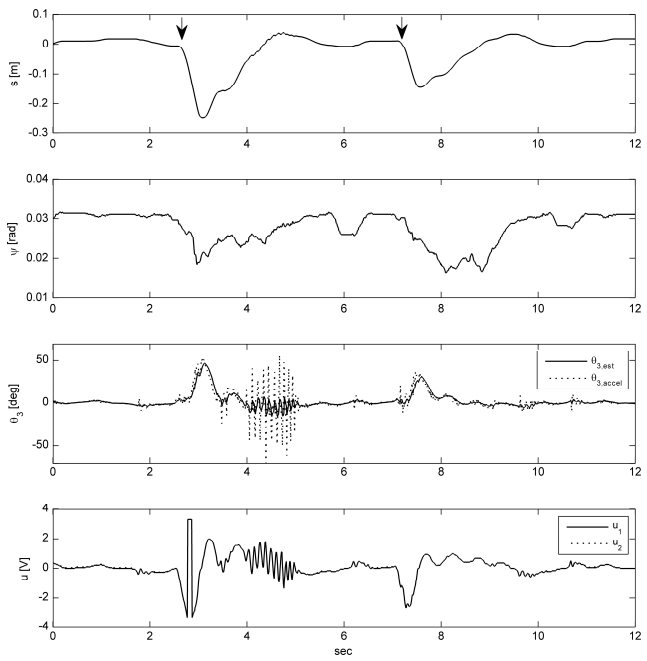

Figure 8. Implementation results. Control performance around the unstable equilibrium point. Dynamic behavior.

was successfully solved. First the robot was pushed about $25\,[cm]$ away while the second time about $15\,[cm]$, the stabilization was achieved approximately in 2.5 seconds.

X. Conclusion And Future Work

In this paper, LQG control strategies were elaborated to a two-wheeled mobile pendulum system. Namely, around the stable equilibrium state of the plant an anti-sway speed controller-, while around the unstable equilibrium point a position controller which ensures the stabilization of the inner body were developed and implemented on the real robot. The asymptotic stability of the closed loop system was proved based on simulation and measurement results. According to the implementation results it is concluded that the elaborated LQG control strategies produce satisfying and competitive control performances. These experiments form our initial results in the investigation of the control performances of different modern control methods. Future work will involve the identification of the unknown parameters, the validation of the developed control strategies and the development of modern (such as nonlinear, fuzzy) control algorithms to the system.

Acknowledgment

We acknowledge the financial support of this work by the Hungarian State and the European Union under the TÁMOP-4.2.2.D-15/1/KONV-2015-0002 project entitled ”Development of Smart technologies for High-tech industry”.

Appendix

The Lagrange function of the system:

$$\begin{aligned}\mathcal{L} = \sum_{i=1}^{2}\left(\frac{3}{4}m_w r^2 + \frac{1}{8}m_b r^2 + \frac{l^2 r^2}{2d^2}m_b \sin^2\theta_3 + \frac{1}{2}J_B\frac{r^2}{d^2} + \frac{1}{2}k^2 J_r\right)\dot{\theta}_i^2 \\ + \sum_{i=1}^{2}\left(\frac{1}{2}m_b l r\cos\theta_3 - k^2 J_r\right)\dot{\theta}_3\dot{\theta}_i \\ + \left(\frac{1}{4}m_b r^2 - \frac{l^2 r^2}{d^2}m_b \sin^2\theta_3 - J_B\frac{r^2}{d^2}\right)\dot{\theta}_1\dot{\theta}_2 \\ + \left(\frac{1}{2}m_b l^2 + \frac{1}{2}J_A + k^2 J_r\right)\dot{\theta}_3^2 - 2m_w g r - m_b g(r - l\cos\theta_3).\end{aligned} \tag{A}$$

Elements of the inertia matrix $M(q) = \left(m_{ij}\right)_{3\times 3}$:

$$\begin{aligned}m_{11} = \frac{3}{2}m_w r^2 + \frac{1}{4}m_b r^2 + k^2 J_r + \frac{l^2 r^2}{d^2}m_b \sin^2\theta_3 + J_B\frac{r^2}{d^2}, \\ m_{22} = m_{11}, m_{33} = m_b l^2 + J_A + 2k^2 J_r, \\ m_{12} = m_{21} = \frac{1}{4}m_b r^2 - \frac{l^2 r^2}{d^2}m_b \sin^2\theta_3 - J_B\frac{r^2}{d^2}, \\ m_{13} = m_{23} = m_{31} = m_{32} = \frac{1}{2}m_b l r\cos\theta_3 - k^2 J_r.\end{aligned} \tag{B}$$

The elements of $V(q,\dot{q}) = (v_1, v_2, v_3)^T$:

$$\begin{aligned}v_1 = 2\frac{l^2 r^2}{d^2}m_b \sin\theta_3\cos\theta_3\,\dot{\theta}_3(\dot{\theta}_1 - \dot{\theta}_2) - \frac{1}{2}m_b l r\sin\theta_3\,\dot{\theta}_3^2, \\ v_2 = 2\frac{l^2 r^2}{d^2}m_b \sin\theta_3\cos\theta_3\,\dot{\theta}_3(\dot{\theta}_2 - \dot{\theta}_1) - \frac{1}{2}m_b l r\sin\theta_3\,\dot{\theta}_3^2, \\ v_3 = -\frac{l^2 r^2}{d^2}m_b \sin\theta_3\cos\theta_3\,(\dot{\theta}_1 - \dot{\theta}_2)^2 + m_b g l\sin\theta_3.\end{aligned} \tag{C}$$

The block matrices of equation (9):

$$\begin{aligned}\tilde{A}_{s,21} = \begin{bmatrix}0 & -0.08\\ 0 & -136.5\end{bmatrix},\ \tilde{A}_{s,22} = \begin{bmatrix}-25.9 & 0.8\\ 2338 & -73.6\end{bmatrix}, \\ \tilde{A}_{s,33} = \begin{bmatrix}0 & 1\\ 0 & -56\end{bmatrix},\ \tilde{B}_{s,2} = \begin{bmatrix}3 & 3\\ -279.6 & -279.6\end{bmatrix}, \\ \tilde{B}_{s,3} = \begin{bmatrix}0 & 0\\ -73.9 & 73.9\end{bmatrix},\ \tilde{C}_{s,2} = \begin{bmatrix}1 & 0\\ 0 & 0\end{bmatrix}, \text{and } \tilde{C}_{s,3} = \begin{bmatrix}0 & 0\\ 0 & 1\end{bmatrix}.\end{aligned} \tag{D}$$

 ISBN: 978-1-61208-437-4

TABLE II. NOTATION OF THE ROBOT PARAMETERS

Symbol	Name	Value [SI Unit]
r	Wheel radius	$3.15 \cdot 10^{-2}$
m_w	Mass of the wheels	$31.6 \cdot 10^{-3}$
l	Distance between the COG and the wheel axle	$8.36 \cdot 10^{-3}$
m_b	Mass of the inner body	$360.4 \cdot 10^{-3}$
d	Distance between the wheels	$177 \cdot 10^{-3}$
$J_{\mathcal{A}}$	Moment of inertia of the inner body about the wheel axle $\mathcal{A}$	$81367 \cdot 10^{-9}$
$J_{\mathcal{B}}$	Moment of inertia of the inner body about the axis $\mathcal{B}$	$574620 \cdot 10^{-9}$
k	Gear ratio	64
J_r	Rotor inertia	$0.12 \cdot 10^{-7}$
R	Terminal resistance	2.3
L	Rotor inductance	$26 \cdot 10^{-6}$
k_M	Torque constant	$2.05 \cdot 10^{-3}$
k_E	Back-EMF constant	$2.05 \cdot 10^{-3}$
b	Viscous friction coefficient between body - motor	$2.1 \cdot 10^{-5}$
f_v	Viscous friction coefficient between wheels - ground	$1.8 \cdot 10^{-4}$

REFERENCES

[1] G. F. Franklin, J. D. Powell, and A. Emami-Naeini, Feedback Control of Dynamic Systems. Pearson Prentice Hall, 2014, ISBN: 978-0-13349-659-8.

[2] A. Divelbiss and J. Wen, "Trajectory tracking control of a car-trailer system," IEEE Transactions on Control Systems Technology, vol. 5, 1997, pp. 269 - 278, doi: 10.1109/87.572125.

[3] O. Araar and N. Aouf, "Full linear control of a quadrotor UAV, LQ vs H∞," UKACC International Conference on Control (CONTROL), 2014, pp. 133 - 138, doi: 10.1109/CONTROL.2014.6915128.

[4] J.-K. Ji and S.-K. Sul, "Kalman filter and LQ based speed controller for torsional vibration suppression in a 2-mass motor drive system," IEEE Transactions on Industrial Electronics, vol. 42, 2002, pp. 564 - 571, doi: 10.1109/41.475496.

[5] S. Bouabdallah, A. Noth, and R. Siegwart, "PID vs LQ control techniques applied to an indoor micro quadrotor," IEEE/RSJ International Conference on Intelligent Robots and Systems (IROS 2004), 2004, pp. 2451 - 2456, doi: 10.1109/IROS.2004.1389776.

[6] S. Jeong and T. Takahashi, "Wheeled inverted pendulum type assistant robot: inverted mobile, standing, and sitting motions," IEEE/RSJ International Conference on Intelligent Robots and Systems (IROS 2007), 2007, pp. 1932 - 1937, doi: 10.1109/IROS.2007.4398961.

[7] S. Zhiyu and L. Daliang, "Balancing control of a unicycle riding," 29th Chinese Control Conference (CCC), 2010, pp. 3250 - 3254, ISBN: 978-1-4244-6263-6.

[8] L. Yi-bo, L. Wan-zhu, and S. Qi, "Improved LQG control for small unmanned helicopter based on active model in uncertain environment," International Conference on Electronics, Communications and Control (ICECC), 2011, pp. 289 - 292, doi: 10.1109/ICECC.2011.6067810.

[9] S. Nagaya, T. Morikawa, I. Takami, and G. Chen, "Robust LQ control for parallel wheeled inverted pendulum," 3rd Australian Control Conference (AUCC), 2013, pp. 189 - 194, doi: 10.1109/AUCC.2013.6697271.

[10] AppL-DSP. Video demonstration of the robot. [Online]. Available from: http://appl-dsp.com/lqg-and-fuzzy-control-of-a-mobile-wheeled-pendulum

[11] A. Salerno and J. Angeles, "A New Family of Two-Wheeled Mobile Robots: Modeling and Controllability," IEEE Transactions on Robotics, vol. 23, 2007, pp. 169 - 173, doi: 10.1109/TRO.2006.886277.

[12] B. Cazzolato et al., "Modeling, simulation and control of an electric diwheel," Australasian Conference on Robotics and Automation (ACRA 2011), 2011, pp. 1-10, ISBN: 978-0-9807-4042-4.

[13] L. Sciavicco and B. Siciliano, Modelling and Control of Robot Manipulators. Springer-Verlag London, 2000, ISBN: 978-1-85233-221-1.

[14] Á. Odry, I. Harmati, Z. Király, and P. Odry, "Design, realization and modeling of a two-wheeled mobile pendulum system," 14th International Conference on Instrumentation, Measurement, Circuits and Systems (IMCAS '15), 2015, pp. 75-79, ISBN: 978-1-61804-315-3.

[15] G. Welch and G. Bishop, "An Introduction to the Kalman Filter," Tech. Rep. TR 95-041, Department of Computer Science, University of North Carolina, USA, 2001.

[16] STMicroelectronics, "Tilt measurement using a low-g 3-axis accelerometer," Application note AN3182, 2010.

 ISBN: 978-1-61208-437-4